Heliyon 9 (2023) e19819

Contents lists available at ScienceDirect

Heliyon

journal homepage: www.cell.com/heliyon

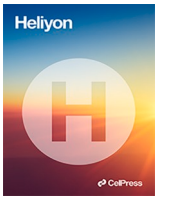

Characterization of an energy efficient pulsed current TIG welding process on AISI 316 and 304 stainless steels

Rosario Casanueva [a,*], Christian Brañas [a], F. Javier Diaz [a], Francisco J. Azcondo [a], Diego Ferreño [b], Jesus Setien [b]

[a] Dept. of Electronics Technology, Systems and Automation Engineering. Universidad de Cantabria, Avda. de los Castros, 46. 39005 Santander, Spain
[b] Laboratory of Science and Engineering of Materials. Universidad de Cantabria, Avda. de los Castros, 44. 39005 Santander, Spain

ARTICLE INFO

Keywords:
Arc welding power supply
Resonant power conversion
Gas tungsten arc welding
Tensile strength
Charpy test

ABSTRACT

This paper presents the characterization of a TIG welding process carried out by means of an arc welding power supply able to provide dc or pulsed current. The arc welding power supply is based on resonant power converters and an FPGA-based control circuit. Dc and multiple pulsed operations up to 1 kHz with different pulse widths have been tested. The operation of the proposed welding power supply has been compared to that of a high-quality commercial welding machine. Regarding performance, the investigated electrical parameters are: power factor, power conversion efficiency and the energy consumption of the process. The radiography and mechanical properties of the welds have been examined. The mechanical properties of the welded joints characterized through tensile tests are the yield stress, tensile strength and the strain under maximum stress. In addition, the impact properties of the joints were determined through Charpy tests and the curves relating energy absorbed and temperature were obtained. The results show an improved performance of the proposed arc welding power supply over the commercial counterpart, with higher efficiency and power factor, as well as lower energy consumption. The yield stress and tensile strength results indicate that the welded plates using pulsed modes with the proposed power supply are comparable to the reference weld performed with dc operation using the commercial welder. Remarkably, it was observed that the ductility of the welded plates using pulsed modes with the proposed power supply outperforms those of the reference weld carried out with dc arc using the commercial welder.

1. Introduction

Tungsten inert gas (TIG) or gas tungsten arc welding (GTAW) is a widely used high-quality, high-precision welding process. In TIG welding, an arc is established between a non-consumable tungsten electrode and the workpiece, which is heated and melted. Filler wire can be used for the weld to provide additional material to the joint. The inert gas shields the welding area preventing oxidation caused by the air, transfers heat (from the electrode to the workpiece) and helps to start and maintain a stable arc, due to the low ionization potential.

The arc is a nonlinear, variable and dynamic electrical load and the design and control of the arc welding power supplies are

* Corresponding author.
E-mail addresses: casanuer@unican.es (R. Casanueva), branasc@unican.es (C. Brañas), diazrf@unican.es (F.J. Diaz), azcondof@unican.es (F.J. Azcondo), ferrenod@unican.es (D. Ferreño), setienj@unican.es (J. Setien).

https://doi.org/10.1016/j.heliyon.2023.e19819
Received 19 January 2023; Received in revised form 2 May 2023; Accepted 1 September 2023
Available online 4 September 2023

oriented to improve the welding quality and the machine performance, providing better arc stability, reducing thermal effects in the metal parts, increasing the penetration and decreasing the spatter.

The design challenges of arc welding machines include minimization of size and weight while increasing efficiency and extension of the duty cycle.

In TIG welding, dc, pulsed dc or ac machines are used. Dc current power supplies provide constant polarity current, resulting in high arc stability. Pulsed dc machines provide current pulses between two current levels: a maximum current level, to melt the base material, and a background current level, to maintain the arc stable. The duration of the current pulses can be changed to weld different thicknesses of the same material, and the current levels are set for each material. Ac TIG welding machines provide a combination of current at both polarities, positive and negative, which is suitable for welding steels and aluminum or its alloys.

Many experimental studies [1–3] address the effects of pulsed current in TIG welding, mostly at low frequencies, with strong influence on the mechanical properties of the welded joint. Pulsed current TIG welding has advantages compared to dc current TIG welding, such as lower heat input, narrower heat affected zone and improved mechanical properties [4] and higher penetration of the weld [5].

Also, in the literature, the impact of pulsing frequency on the microstructure and mechanical properties of welded joints has been extensively investigated for various materials and conditions. In a recent study by Madhusudhan et al. [6], the effects of current pulsation frequency on the microstructure, hardness, and tensile properties of an AA8090 type aluminum-lithium alloy were characterized. The authors found that the grain structure became finer and more equiaxed with the introduction of current pulsation, leading to an optimal combination of harness and tensile strength. Specifically, the best combination of tensile properties was achieved for welds deposited under a 6 Hz pulse frequency. In a separate study, Madhusudhan et al. [7] conducted an experimental investigation to evaluate the influence of the welding technique on the microstructure and the pitting corrosion resistance of an aeronautical grade Al–Li based alloy. The authors observed that the welding technique had a significant impact on the microstructure, and the resultant pitting corrosion resistance. Specifically, the welding technique led to a more refined and uniform microstructure, resulting in improved pitting corrosion resistance of the Al–Li based alloy. Shelwatker et al. [8] conducted a study to investigate the weldability of two high strength aluminum alloys using conventional and pulsed gas tungsten arc welding. The authors evaluated the solidification cracking tendency, microstructure, tensile properties, and microhardness across the welds. The authors found improved mechanical properties in pulsed welds compared to conventional welding, which were related to the refinement of the fusion zone microstructure. In addition, Mohandas and Madhusudhana [9] investigated the influence of pulse frequency in gas tungsten arc welding on grain size and morphology in titanium alloys. The authors observed that the pulse frequency has a significant influence on the grain size and morphology of the fusion zone, which contradicted the observations made by other authors. These differences were attributed to the different frequency band and current combinations investigated. The authors emphasized the need for further research to understand the influence of various pulsing variables on the fusion zone grain size and its corresponding influence on the mechanical properties of titanium alloy welds. Overall, these studies suggest that the pulsing frequency and welding technique can significantly influence the microstructure and mechanical properties of welded joints, and careful selection of these parameters can lead to improved performance of welded components.

Several studies have been conducted on the application of pulsed current techniques in stainless steel welding, examining their impact on microstructural features and mechanical properties. Two recent studies, by Tabrizi et al. [10] and Sabzi et al. [11], have investigated the effects of continuous and pulsed current in the GTAW process of AISI 316L stainless steel welded joints. The results of these studies indicate that changing the welding current from continuous to pulsed mode led to a change in the weld metal morphology of the grains from elongated columnar to equiaxed and a substantial reduction in the grain size. Furthermore, this change in the welding process resulted in a significant increase in hardness and absorbed energy (fracture energy) of the weld metal. In a similar study, Sabzi et al. [12] investigated the effect of pulse current changes in Pulsed Current GTAW on microstructural and mechanical properties of dissimilar welds of AISI 316L – AISI 310S stainless steels. The authors reported a reduction in dendrite size when the background current was increased and the peak current was decreased. These microstructural changes were linked to a significant improvement in mechanical properties, as evidenced by tensile test analysis, which indicated that the strength of the weld metal in the welded joints was higher than the strength of the base metals. Moreover, all the welded joints were broken from the AISI 316L side during tensile tests. Furthermore, the hardness of the weld metal increased substantially from 270 HV to 318 HV, and the fracture energy from Charpy impact test showed an even more pronounced increase from 153 J to 198 J when the background current was increased and peak current decreased.

Present-day arc welding power supplies are mostly based on inverter technology, that is, a full-bridge inverter, a transformer and a full wave rectifier stage. Advanced contributions for inverter-based power stages oriented to increasing the power conversion efficiency and the dynamic response are found in Ref. [13], proposing a sliding control mode for a dc arc welding inverter power source based on a phase-shift full-bridge soft switching inverter. In Ref. [14], the design and implementation of a zero-voltage-zero-current switching full-bridge dc/dc converter with phase-shifting PWM in a dc arc welding machine application is presented. The interaction of the pulsed modes and the grid impedance may cause distortion of the utility voltage and affect the grid quality. In Ref. [15], a power conversion system for a dc or pulsed arc welding process composed of a power factor corrector (PFC) boost converter is presented to comply with the grid standards and a full-bridge phase-shift zero-voltage-switching converter. In the pulsed operation mode, the current is regulated by an active current controller. In Ref. [16], an ac TIG welding equipment is proposed with four power conversion stages, two with active control: ac-dc input rectifier, high-frequency dc-ac power inversion by means of a full bridge inverter, high-frequency ac-dc rectification and a low-frequency dc-ac current inverter to obtain a regulated ac output current. An ac arc welding power supply in which the center-tapped transformer is replaced by two current doubler rectifiers with two coupled inductors reducing the current stress in the magnetic parts is proposed in Ref. [17]. The full-bridge converter supplies energy to a final

half-bridge stage to obtain a square ac output current.

The optimization of use of renewable energy has been addressed through several methods including maximum power tracking algorithm [18], power factor correction stage based on a bridgeless SEPIC converter for improved grid quality [19] and generation of low frequency pulsed current using line switched devices [20].

In this paper, it is proposed to leverage the properties of high-frequency resonant converters to apply this technology in the control of discharges, including arc welding, because they enable implementation of small-size, light-weight, and high-efficiency systems along with additional inherent arc stability.

The contributions of this work are summarized in the following points:

- Using high frequency power electronics conversion technique to achieve fast dynamic response of the welding arc and then more flexible and adaptable pulsed TIG process.
- By including a front-end power factor correction stage, not only the quality of the grid current is improved but also indirectly stabilize the welding arc. This is because the arc forming power converter, which is a resonant converter, operates in open loop and increases robustness.
- Providing energy measurements and mechanical tests that show that the proposed pulsed current power supply, based on resonant converters, achieves better quality vs. energy consumption trade-off and better energy efficiency. The welding quality is equivalent in most of the tests and higher in some of them compared to a commercial machine based on microprocessor controlled non-resonant inverter power sources.

The experimental scope of this study is based on the fabrication of welded joints of plates of stainless steels AISI 316 and AISI 304.

To the best knowledge of these authors, no other previous study has addressed the use of new capabilities of power electronic devices to achieve faster dynamics of the arc to improve the performance of TIG welding technology using the properties of resonant converters for proper arc stabilization with no-closed loop control while enabling a fast modulation of the arc current.

In this study, an exhaustive characterization of the mechanical and impact properties of the welded joints was carried out through tensile and Charpy tests to establish a fair comparison. The tensile tests provided information on yield stress, tensile strength, and strain under maximum stress, while the Charpy tests determined the impact properties of the joints and obtained curves relating energy absorbed as a function of temperature. The results of the mechanical and impact tests were used to evaluate the performance of the proposed TIG welding process and compare it to that of the commercial welding machine. The characterization of the welded joints provided a detailed understanding of the effects of the welding process on the mechanical and impact properties of the welded joints, which is essential for the development of efficient and reliable welding technologies.

The paper is organized as follows. Section II describes the arc welding power supply, the proposed control of the resonant inverter and the current modulation capabilities in open loop to provide the different operation modes. Section III summarizes the arc welding test setup and procedure. Section IV presents and discusses the experimental results through energy measurements and both radiographic and mechanical tests, finalizing with conclusions.

2. Description of the power supply and the proposed control

The proposed arc welding power supply is designed following a modular structure, as shown in Fig. 1 [21], which enables the welding current to be scaled up by adding modules. Each module consists of two parallel connected LC_sC_p resonant converters, supplying up to 50 A. The dc input voltage for each resonant converter is obtained from a PFC circuit based on a boost converter, which ensures the stability of the dc link voltage.

The basic LC_sC_p resonant converter building block [22] is shown in Fig. 2.

The LC_sC_p resonant converter is designed to achieve an intrinsic, and therefore robust, current source behavior [23]. The behavior

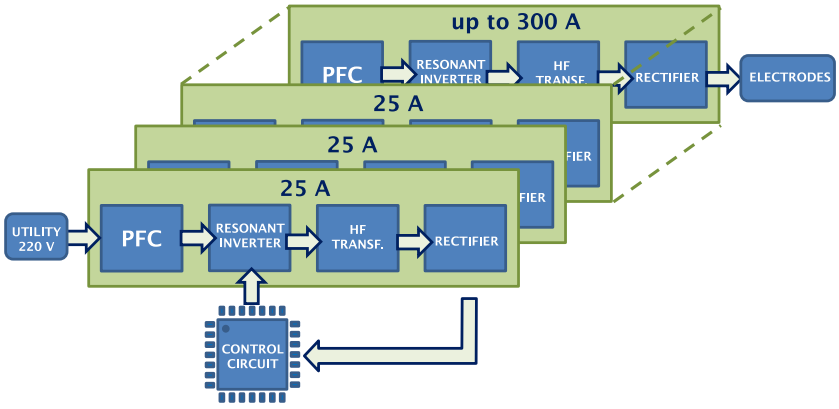

Fig. 1. Modular architecture of the arc welding power supply.

as a current source is inherent to the circuit if the switching frequency is equal to the natural resonant frequency, ω_o [24].

$$\omega_o = \omega_p \sqrt{1 + C_p/2C_s} \tag{1}$$

Working at ω_o, the output current value, I_o, is defined by (2) [24], where Ψ is the angle of phase displacement between the midpoint voltages of branches A and B of the converter, used as a current modulation parameter.

$$I_o = \frac{nV_{dc}\sqrt{1 + C_p/2C_s}}{Z_p} Cos(\Psi/2) \tag{2}$$

Each converter, i.e. half of the module, is designed to supply the maximum output current, $I_o = 25$ A. The parallel characteristic impedance, Z_p, is calculated from (2), once the transformer turn ratio, n, the input dc voltage, V_{dc}, and the capacitor ratio $C_p/2C_s$ are known. The parameters of the converter are summarized in Table 1.

Varying Ψ from 0° to 180°, the output current is controlled from its maximum value down to zero, while keeping the switching frequency constant.

2.1. Control of the resonant converter

Leveraging the current source behavior of the converter, a control loop for stabilizing the arc current is avoided. The open loop operation brings on the fast-dynamic response of the converter enabling the implementation of pulsed modes of welding at high frequency.

The digital control circuit achieves a resolution higher than 1% in the variation range of Ψ with eight bits. Taking into account the desired operation mode (dc welding or pulsed mode) and the necessary welding current, the control circuit defines the required value of modulation angle, Ψ at each instant.

The core of the control circuit is a state machine which calculates the value of Ψ from the comparison between a high-frequency digital signal *c[7..0]* (carrier) with a low-frequency signal *m[7..0]* (modulator). Typical waveforms are depicted in Fig. 3.

Ph1 and *Ph2* are the control signals for the transistor's branches A and B of each resonant converter. All modules share the same control signals, working synchronously.

2.2. Dc welding

The dc welding is carried out by adjusting Ψ according to the maximum value of current demanded by the welding process. During the welding process, the value of Ψ can be kept constant or it is possible to implement a continuous variation according to (2).

2.3. Pulsed mode

This mode is implemented with two values of Ψ, according to required maximum and minimum values of welding current. Although the current can be totally cancelled out by setting Ψ = 180°, a minimum value of 10% is stablished in order to avoid arc cooling and extinguishing. The timing for maximum current "on" and minimum current "off" as well as the frequency are controlled by a pulse-width modulated (PWM) signal.

3. Welding test setups

Practical TIG welding operations have been carried out. The current-mode operation requires overvoltage protection that has been set at 48 V. The present study details the execution of manual TIG welding utilizing a 2.4-mm diameter tungsten electrode. The welding

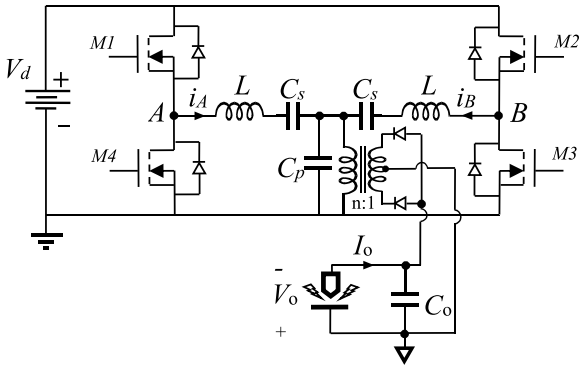

Fig. 2. Phase controlled LC_sC_p resonant converter.

Table 1
Parameters of the LC_sC_p resonant converter.

V_{dc}	I_o	n	ω_o	L	C_p	C_s
400 V	25 A	11	2π(125 kHz)	230 μH	17.2 nF	80 nF

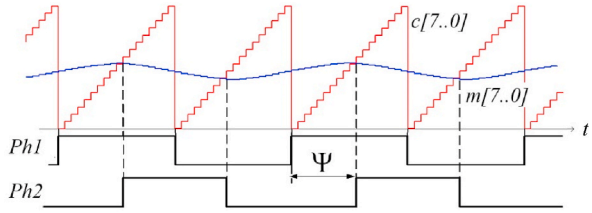

Fig. 3. Digital waveforms for implementing the phase control.

operation is performed on stainless steel plates of two distinct grades, AISI 316 and AISI 304, the dimensions of which are dependent on the experimental setup. The weld configuration adopted in this investigation is the V joint, a widely recognized weld joint used for optimal penetration and weld quality. Welding is conducted using both non-pulsed and pulsed current TIG welding.

TIG welding of materials up to 3 mm thick does not require filler material while multi-pass welding with filler material is required to weld thicker parts [25].

In manual TIG welding, the operator moves the torch in the direction of the welding, maintaining the arc. The shielding gas is pure argon and filler material is used during the welding experiments. The argon is supplied at a constant flow rate of 12–14 L/min.

The setups and specimens are designed to accomplish the requirements of the test methods described by the standards ASTM E8/E8M−16 [26] and ASTM E23-16 [27] to perform tensile and Charpy tests, respectively.

Table 2 and Table 3 summarize the welding parameters used in the provision of the test welds on AISI 316 and AISI 304 stainless steels, respectively. Weld joints corresponding to the setup shown in Table 2 required a mean value of twenty-four passes and, in the case of those carried out according to the setup summarized in Table 3, seven passes were required.

AISI 304 is widely recognized as the most commonly used stainless steel owing to its high versatility within the austenitic grades. This chromium-nickel steel alloy is typically employed in a wide range of household and industrial applications such as food handling and processing equipment, screws, machinery parts, utensils, and exhaust manifolds. Moreover, 304 stainless steel is frequently used in architectural settings for exterior embellishments such as water and fire features, and it is also a popular material for vaporizer coils. The typical mechanical properties of AISI 304 in the annealed condition are: Brinell, hardness, 123; yield stress, 215 MPa; tensile strength, 515 MPa. Alloy 316 is a chromium-nickel-molybdenum austenitic stainless steel engineered to provide enhanced corrosion resistance compared to alloy 304 in moderately corrosive environments. Its molybdenum content serves to improve general corrosion and chloride pitting resistance while also providing higher creep, stress-to-rupture, and tensile strength at elevated temperatures. Thus, it is frequently utilized in process streams containing chlorides or halides, and it is particularly suited for applications in which corrosion resistance is a primary concern. The specified chemical compositions of both plate materials are described in Table 4. The typical mechanical properties of AISI 316 in the annealed condition are the following: Brinell, hardness, 149; yield stress, 205 MPa; tensile strength, 515 MPa [28].

4. Experimental results

The proposed control circuit has been synthesized in a Xilinx Spartan 3 FPGA (XC3S200) and the chosen power converter switching frequency is 125 kHz. In reference to the schematic shown in Fig. 2, the inverter MOSFETs are STB25NM50 N, the MOSFET drivers are IR2113S and the output power Schottky diodes are DSS 2X101-015A.

Table 2
Welding parameters used in the tests. Setup 1.

Parameter	Setup 1
Plate dimensions	200 mm × 75 mm × 10 mm
Plate material	AISI 316
Separation between plates	12 mm
Electrode	Tungsten
Electrode diameter	2.4 mm
Filler metal	AISI 316L
Filler diameter	2.4 mm
Polarity	Negative
Shielding gas	Argon
Flow rate	12–14 L/min

Table 3
Welding parameters used in the tests. Setup 2.

Parameter	Setup 2
Plate dimensions	250 mm × 10 mm × 8 mm
Plate material	AISI 304
Separation between plates	2–4 mm
Electrode	Tungsten
Electrode diameter	2.4 mm
Filler metal	AISI 308
Filler diameter	2.4 mm
Polarity	Negative
Shielding gas	Argon
Flow rate	12–14 L/min

Table 4
Chemical compositions (weight %) of AISI 304 and AISI 316 stainless steels (all values are maximum unless a range is otherwise indicated) [28].

Element	AISI 304	AISI 316
Cr	18.0–20.0	16.0–18.0
Ni	8.0–10.5	10.0–14.0
Mo	–	2.00–3.00
C	0.08	0.08
Mn	2.00	2.00
P	0.045	0.045
S	0.03	0.03
Si	0.75	0.75
N	0.1	0.1
Fe	Balance	Balance

Different pulsed TIG welding experiments have been performed in which there are abrupt profiles of the arc current pulses. These profiles are a consequence of the good dynamic response of the proposed power supply. Dc arc welding and pulsed mode operations up to 1 kHz with different pulse widths have been carried out. The power factor correction stage has the function of maintaining the power factor close to unity and stabilizing the input voltage to the resonant converter, which in turn provides stability to the arc current. Fig. 4 shows the measured efficiency, η (Fig. 4a), and power factor, PF (Fig. 4b), for a commercial inverter arc welding power supply, a Fronius MagicWave 3000 TIG welding machine, and the proposed power supply for different operation modes: dc and 40 Hz, 250 Hz, 500 Hz and 1 kHz pulsed current with 50% on time. The operations have been set at a 150 A output current for dc operation and a 150 A high level current in the case of pulsed operation.

The arc voltage and current are monitored with an oscilloscope. The arc-voltage waveform is monitored directly between the tungsten electrode and metals to be welded. A Pacific 345-AMX linear power source has been used for the power supply of the arc welding machines, along with the Universal Protocol Converter (UPC) Manager control and data analysis software with which the data used for the analysis, such as power factor and input power, are obtained.

From the results in Fig. 4, it follows that the efficiency and PF are, in all cases, better for the case of the proposed arc welding power supply compared to the commercial one used as a reference. In the best case, up to 26% in efficiency improvement is achieved.

The arc voltage (bottom) and current (top) waveforms with a duty cycle of 75% for TIG welding are shown in Fig. 5. The corresponding pulsed power supply frequency is 40 Hz in Figs. 5a and 500 Hz in Fig. 5b. The pulse current is ~150 A and the background current is ~20 A.

Heat input is a relative measure of the energy transferred during the welding process. It is a significant characteristic because it may affect the mechanical properties and metallurgical structure of the weld. Heat input is calculated as the ratio H=(V.I)/S [29], where H is the heat input (J/mm), V is the arc voltage (V), I is the welding current (A) and S is the welding speed (mm/s). This parameter is suitable for properly comparing different welding procedures for a given process, in this case TIG welding [29].

The welding process has been analyzed for the test welds and welding conditions shown in Tables 5 and 6. The welding beads result from a similar heat input per unit length of weld.

Fig. 6 shows photographs of a selection of the welds carried out corresponding to the pulsed mode at 40 Hz, 75% and 250 Hz, 75%.

The energy consumption data in kWh of the welds have been analyzed and the results are shown in Tables 7 and 8 for Setup 1 and 2, respectively.

For Setup 1, the same weld in dc operation performed by the studied machine results in lower energy consumption than with the commercial machine. In the best case, a reduction of the energy consumption of up to 49% is obtained with the proposed arc welding power supply. It is also observed that in case of the same weld with the pulsed modes, the energy consumption is lower compared to the dc operation mode and also decreases as the frequency of the pulses increases.

For Setup 2, the same tendency is observed up to 500 Hz, at which frequency the results show the minimum energy consumption.

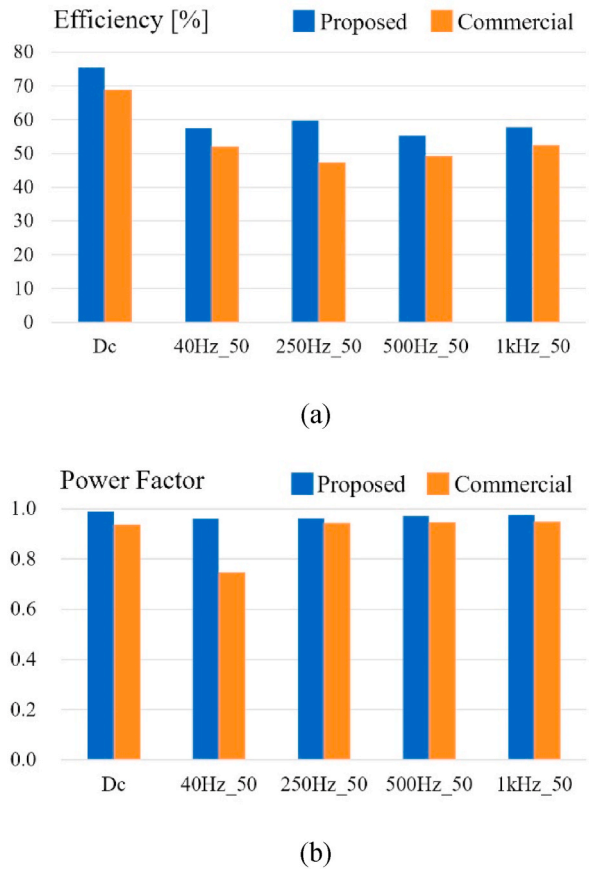

Fig. 4. Measured η and PF comparison: proposed and commercial welding machine for different operation modes: (a) efficiency, (b) power factor.

4.1. Radiographic observations

After the welding process, the resultant weld joints were subjected to radiography to assess the internal quality of the welds and to detect any potential defects. Fig. 7 depicts the results of the radiographic analysis, which indicates that the welds exhibit no discernible defects such as pores, cracks, slags, lack of fusion, lack of penetration, undercuts, shrinkages, among others. These results confirm that the weld quality of the joints is deemed satisfactory, and that the welding process employed in this study can produce structurally sound weld joints.

4.2. Mechanical tests

The mechanical performance of the welds was assessed by means of two complementary experimental techniques, tensile tests and Charpy impact tests. Tensile tests were carried out with an Instron universal servo-hydraulic testing machine, model 8501, with a loading capacity of 100 kN. The tests have been carried out following the specifications of ASTM E8/E8M-16a [26], at room temperature (20 ± 2 °C). In all cases, quasi-static and control of displacement conditions have been imposed, applying a test rate of 1 mm/min. Strains have been measured in real time using a contact extensometer. The yield stress, tensile strength and strain under maximum load have been obtained. Two tensile specimens were obtained from each welded plate.

Charpy tests were carried out by means of an AMSLER RKP300 machine on standardized V-notched Charpy specimens, following the standard ASTM E23-16b [27]. The tests were performed in a wide range of temperatures, in order to ascertain their influence on the material toughness. Since the thickness of the welded plates is not uniform for Setup 1 and Setup 2, the energy absorbed per unit area at fracture was determined in the tests. Seven specimens were machined from each of the available plates.

The outcomes derived from the tensile tests conducted on the weld joints are collated in Table 9 and represented in Fig. 8. As can be seen, the mechanical properties obtained, represented by the yield stress and the tensile strength are in all cases clearly higher than the reference properties of AISI 304 and AISI 316 alloys. It is important to note that Setup 1, which includes conditions P3 and P4, was carried out utilizing a pulsed current TIG welding process, while condition P1 was performed using a dc commercial welder and serves as the reference. From Table 9, it can be observed that the yield stress of condition P1 (417 ± 4 MPa) is marginally greater than those of the experimental conditions, P3 and P4 (394 ± 14 MPa). However, no significant disparities were observed in the tensile strength (618

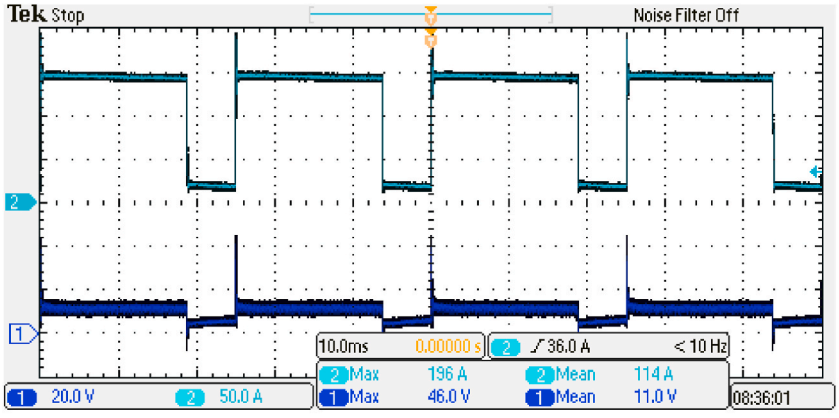

(a)

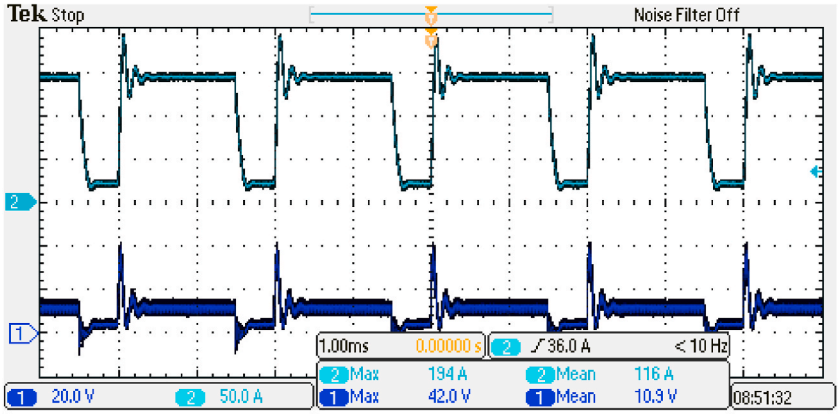

(b)

Fig. 5. Arc voltage (ch1) and current (ch2) waveforms for TIG welding: (a) 40 Hz, 75%, time scale: 10 ms/div and (b) 500 Hz, 75%, time scale: 1 ms/div.

Table 5
Welding conditions of test welds. Setup 1.

ID	Mode	Heat Input (kJ/mm)
P1	Dc commercial welder	0.65
P3	Proposed pulsed 40 Hz 75%	0.67
P4	Proposed pulsed 250 Hz 75%	0.66

Table 6
Welding conditions of test welds. Setup 2.

ID	Mode	Heat Input (kJ/mm)
	Dc proposed welder	0.67
P7	Proposed pulsed 1 kHz 75%	0.62
P8	Proposed pulsed 130 Hz 75%	0.65
P9	Proposed pulsed 500 Hz 75%	0.56
P10	Proposed pulsed 500 Hz 50%	0.53

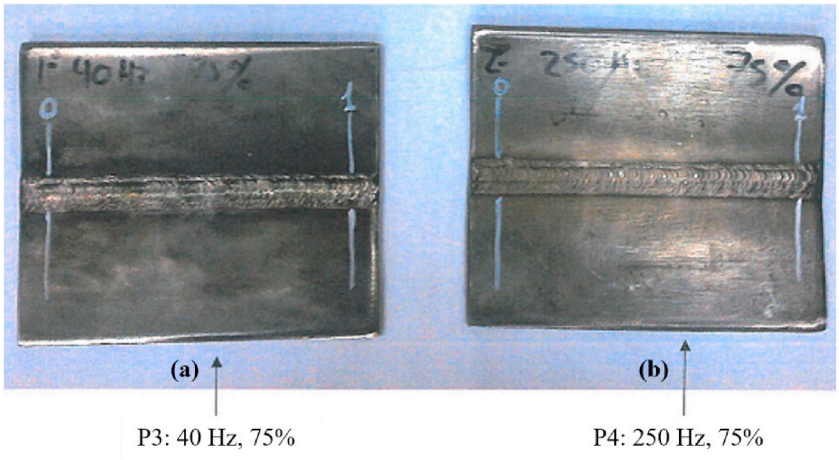

Fig. 6. Photographs of weld bead: (a) 40 Hz, 75% and (b) 250 Hz, 75%.

Table 7
Energy consumption, kWh. Setup 1.

Mode (ID)	Energy Consumption (kWh)
Dc commercial welder (P1)	2493.37
Dc proposed welder	1919.76
Proposed pulsed 40 Hz, 75% (P3)	1372.04
Proposed pulsed 250 Hz, 75% (P4)	1273.41

Table 8
Energy consumption, kWh. Setup 2.

Mode (ID)	Energy Consumption (kWh)
Dc proposed welder	507.64
Proposed pulsed 130 Hz, 75% (P8)	478.61
Proposed pulsed 500 Hz, 75% (P9)	429.00
Proposed pulsed 1 kHz, 75% (P7)	487.61

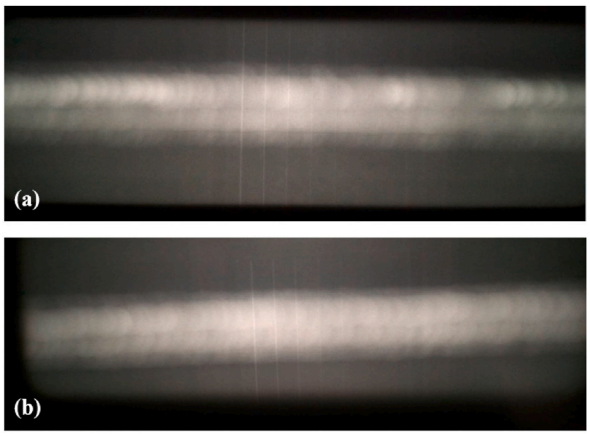

Fig. 7. X-ray radiography images of the weld joints: (a) 40 Hz, 75% and (b) 250 Hz, 75%.

$\pm$ 1 MPa for condition P1, and 618 $\pm$ 16 MPa for conditions P3 and P4). The most noteworthy divergence is evident in the strain under maximum stress, wherein the ductility of the experimental group (24 $\pm$ 2%) notably surpasses that of the reference condition (13 $\pm$ 2%). These findings suggest that the pulsed current TIG welding process is capable of producing weld joints with superior ductility

Table 9
Summary of results obtained from the tensile tests.

Setup	Specimen	Yield stress (MPa)	Tensile strength (MPa)	Strain under maximum load (%)
Setup 1	**P1.1**	419.8	618.9	14.5
	P1.2	414.3	616.8	12.2
	P3.1	390.3	627.6	23.7
	P3.2	409.8	633.4	21.6
	P4.1	399.1	597.0	22.5
	P4.2	377.7	614.2	26.4
Setup 2	**P7.1**	355.7	593.9	34.2
	P7.2	299.1	593.2	25.9
	P8.1	331.9	615.8	37.6
	P8.2	392.2	592.4	28.5
	P9.1	311.6	603.4	22.3
	P9.2	484.8	620.4	36.9
	P10.1	343.8	601.7	34.1
	P10.2	351.1	576.7	27.8

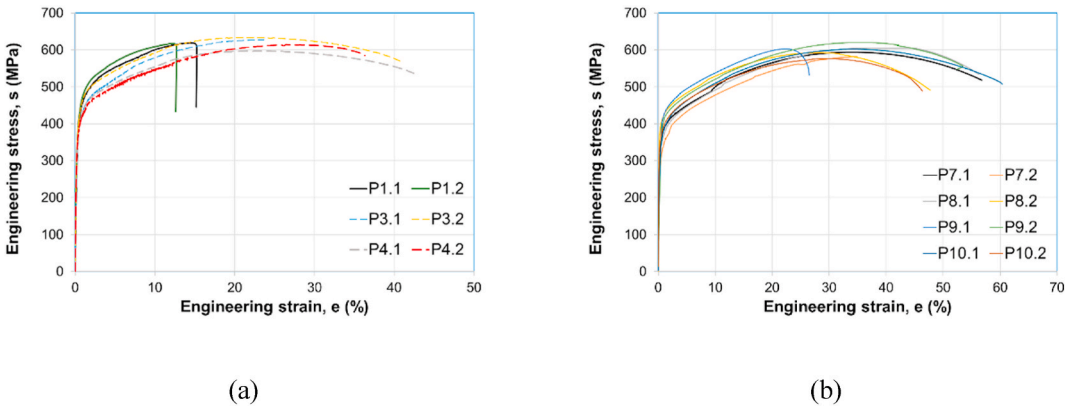

Fig. 8. Engineering stress vs. strains curves obtained in the tensile tests: (a) Setup 1 and (b) Setup 2.

compared to those obtained through traditional welding techniques.

Regarding Setup 2, no reference welding condition is available, and due to the difference in plate sizes from Setup 1, it would be invalid to utilize the results of group P1 as a reference. Consequently, the analysis of the tensile test results for Setup 2 is limited to the comparison of their mechanical parameters. The comparison of the results for groups P7, P8, and P9 enables the effect of the welding frequency to be examined. However, no significant differences in any of the mechanical properties are apparent, apart from the intrinsic scattering of the results. The yield stress for conditions P7, P8, and P9 are respectively 327 $\pm$ 40 MPa, 362 $\pm$ 43 MPa, and 398 $\pm$ 122 MPa, while the tensile strength values are 594 $\pm$ 1 MPa, 604 $\pm$ 17 MPa, and 612 $\pm$ 12 MPa, respectively. Similar results are obtained when comparing the values obtained for condition P10 (D = 50%) with P7, P8, and P9 (D = 75%). For condition P10, the yield stress is 347 $\pm$ 5 MPa, the tensile strength is 589 $\pm$ 17 MPa, and the ductility is 31 $\pm$ 4%. These observations suggest that the welding frequency has minimal effect on the mechanical properties of the weld joints, as demonstrated by the similarity of the results for different welding frequencies.

To statistically compare the results of the tensile tests for the different groups, the one-way ANOVA test [30] is utilized. This method tests the hypothesis that the samples were drawn from populations with the same mean against the alternative hypothesis that the population means are not all the same. The p-values are presented in Table 10, and at the 0.05 significance level, the means are only different for the strain under maximum load in Setup 1. This observation corresponds well with the data provided in Table 9, which indicates that the ductility of the samples from groups P3 and P4 is significantly higher than that of group P1. Furthermore, the statistical analysis indicates that there are no significant differences for the other mechanical properties. These findings suggest that, apart from the ductility, the mechanical properties of the weld joints for different groups are similar, as indicated by the lack of statistical significance at the 0.05 level in the p-values.

The energy absorbed per unit area in the Charpy test is illustrated in the graphs depicted in Fig. 9, where Fig. 9a corresponds to the specimens from Setup 1, and Fig. 9b includes the results of Setup 2. The plots reveal that, in all cases, some degree of embrittlement is observed as the temperature decreases, which is a common characteristic of steels, more pronounced in ferritic grades than in austenitic ones such as AISI 304 and AISI 316. In order to describe this trend, the data are fitted using the hyperbolic tangent model of equation (3) [31]. The fitting parameters, denoted by A, B, C, and D, are obtained from the fitting procedure.

Table 10
Summary of results obtained from the ANOVA test.

Setup	Property	p-value
Setup 1	Yield stress	0.201
	Tensile strength	0.098
	Strain under maximum load	0.023
Setup 2	Yield stress	0.841
	Tensile strength	0.430
	Strain under maximum load	0.960

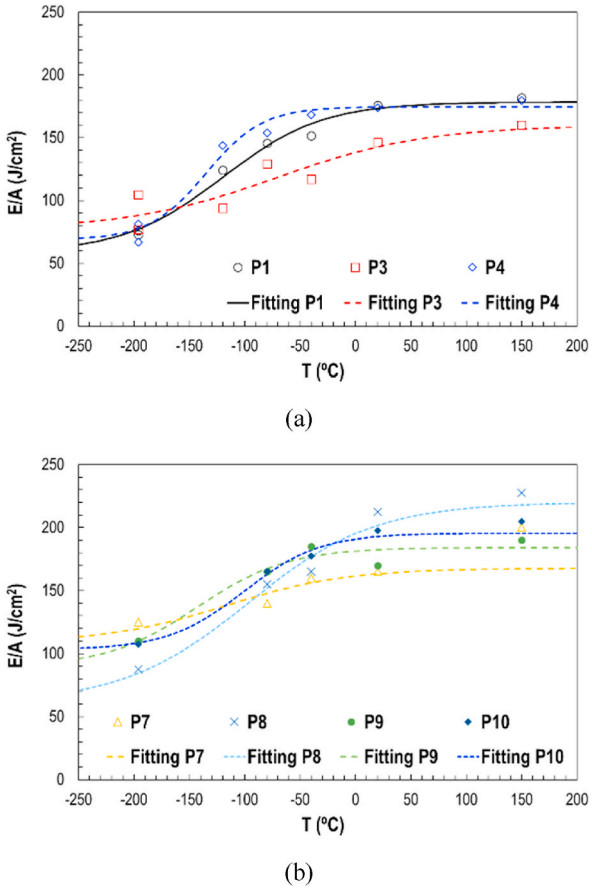

Fig. 9. Energy absorbed per unit area in the Charpy test: (a) Setup 1 and (b) Setup 2.

Table 11
Upper shelf energy and the transition temperature.

		USE (J/cm2)	Ttr (°C)
Setup 1	**P1**	178.37	−120.00
	P3	159.74	−70.49
	P4	174.58	−135.00
Setup 2	**P7**	167.70	−116.50
	P8	220.05	−96.63
	P9	184.12	−143.20
	P10	195.54	−100.90

$$E = A + B \bullet Tanh\left(\frac{T - C}{D}\right) \quad (3)$$

These fittings make it possible to estimate the Upper Shelf Energy as well as the Transition Temperature. These results are shown in Table 11. With regards to Setup 1, it is observed that condition P4 is able to match the results obtained with the reference condition, P1. In contrast, condition P3 offers a slightly lower Charpy toughness, at least in the range of temperature between −150 °C and 150 °C. Note that, in all cases the material shows a tough response at high temperature (see the values of the Upper Shelf Energy) as well as a reduced value for the Transition Temperature. It is difficult to establish any definitive conclusion about Setup 2 since the scatter of results masks the possible differences existing between groups. In spite of this, the results shown in Table 10 allow the same considerations to be established: the welds belonging to Setup 2 show high toughness throughout the temperature range which is represented by a high value for the Upper Shelf Energy and a reduced value of the Transition Temperature.

5. Conclusions

A power supply built with dual-phase resonant converter blocks, designed to maximize the output impedance, has been proposed to operate as an input voltage dependent current source, with the input voltage stabilized by a previous front-end power factor correction stage and the output current modulated by the overlap angle between the voltages of each phase.

The performance of the resulting prototype has been compared with a high-quality commercial welding machine. The fast-dynamic response of the output current vs. the control signal of the proposed power supply has been used to generate pulsed-arc modes.

The effect of the pulsed modes on the welding quality using standardized parts has been studied through energy measurements and mechanical and radiographical tests, showing that pulsed-arc modes achieve a better quality vs. energy consumption tradeoff and the proposed power supply achieves better energy efficiency in the welding process, while the welding quality is comparable in most cases and in some tests even better.

The experimental results show better performance of the proposed arc welding power supply compared to the commercial one used as reference, in the best case:

- An increase of up to 26% in efficiency is achieved (measured for a pulse amplitude of 150 A, frequency of 250 Hz and 50% on time case).
- An increase of up to 28% in the power factor is achieved (measured in both, Setup 1 and Setup 2 cases).
- A reduction of the energy consumption of up to 49% (measured in Setup 1 case)

The tensile tests carried out measured material parameters such as yield stress, tensile strength, and ductility. The results show that the yield stress and tensile strength of the pulsed current TIG welding process are comparable to those of the reference condition using a dc commercial welder while their ductility notably exceeds it. Moreover, the mechanical properties of the weld joints for different frequencies are similar, as indicated by the lack of statistical significance at the 0.05 level in the p-values. In this sense, the study concludes that the pulsed current TIG welding process is capable of producing weld joints with superior ductility compared to those obtained through traditional welding techniques, and that the welding frequency has minimal effect on the mechanical properties of the weld joints.

In addition, the present study investigated the Charpy impact behavior of specimens fabricated using the pulsed current TIG welding process and compared it with the response obtained with the dc commercial welder. The energy absorbed per unit area in the Charpy test was analyzed for both sets of specimens and revealed that the material exhibited a tough response at high temperatures with a reduced value for the Transition Temperature. The findings indicate that the specimens fabricated through the pulsed current TIG welding process were able to match the response obtained with the dc commercial welder. These results are promising and suggest that the pulsed current TIG welding process could be a viable alternative to the dc commercial welding process for applications requiring high toughness at elevated temperatures.

In future work, new technologies such as wide bandgap devices will be used, which result in a reduction of both the switching transient time and on resistance. This advancement will significantly improve the ability of resonant converters to process higher power levels at higher frequencies achieving even steeper arc current transients with more compact power converters.

Author contribution statement

Rosario Casanueva: Diego Ferreño: Conceived and designed the experiments; Performed the experiments; Analyzed and interpreted the data; Wrote the paper.

Christian Brañas: Francisco J. Azcondo: Conceived and designed the experiments; Analyzed and interpreted the data; Wrote the paper.

F. Javier Diaz: Performed the experiments; Analyzed and interpreted the data; Wrote the paper.

Jesús Setién: Performed the experiments; Contributed reagents, materials, analysis tools or data; Wrote the paper.

Data availability statement

Data will be made available on request.

Declaration of competing interest

The authors declare that they have no known competing financial interests or personal relationships that could have appeared to influence the work reported in this paper.

Acknowledgements

This work was supported by the Spanish Government and the EU through the projects RTI2018-095138-B-C31: "Power Electronics for the Grid and Industry Applications" and PID2021-128941OB-100: "Efficient Energy Transformation in Industrial Environments".

Authors acknowledge Luis San Segundo and Xabier Mediavilla from DEGIMA S. A. for their valuable technical support.

References

[1] J. Scemeliovas, Determination of pulse current optimal parameters for manual arc welding, Mechanika 51 (2005) 66–69.
[2] A. Traidia, F. Roger, E. Guyot, Optimal parameters for pulsed gas tungsten arc welding in partially and fully penetrated weld pools, Int. J. Therm. Sci. 49 (2010) 1197–1208, https://doi.org/10.1016/j.ijthermalsci.2010.01.021.
[3] T.V. Cunha, A.L. Voigt, C.E. Niño-Bohórquez, Analysis of mean and RMS current welding in the pulsed TIG welding process, J. Mater. Process. Technol. 231 (2016) 449–455, https://doi.org/10.1016/j.jmatprotec.2016.01.005.
[4] Z. Tong, Z. Zhentai, Z. Rui, A dynamic welding heat source model in pulsed current gas tungsten arc welding, J. Mater. Process. Technol. 213 (12) (2013) 2329–2338, https://doi.org/10.1016/j.jmatprotec.2013.07.007.
[5] M. Arivarasu, K. Devendranath Ramkumar, N. Arivazhagan, Comparative studies of high and low frequency pulsing on the aspect ratio of weld bead in gas tungsten arc welded AISI 304L plates, Procedia Eng. 97 (2014) 871–880, https://doi.org/10.1016/j.proeng.2014.12.362.
[6] G. Madhusudhan Reddy, P. Sammaiah, C.V.S. Murty, T. Mohandas, Influence of welding techniques on microstructure and mechanical properties of AA 6061 (Al-Mg-Si) GTA Welds, Proceed Int Weld Conf (1999) 33–46.
[7] G. Madhusudhana Reddy, Studies on the Application of Pulsed Current and Arc Oscillation Techniques on Aluminum-Lithium Alloy Welds, 1998. PhD Thesis, 11T-Madras.
[8] D.A. Shelwatker, G. Madhusudhan Reddy, A.A. Gokhale, Gas Tungsten Arc Welding Studies on Similar and Dissimilar Combinations of Al-Zn-Mg Alloy RDE 40 and Al-Li Alloy 1441, Science and Technology of welding and Joining, 2002, pp. 352–361.
[9] T. Mohandas, R.G. Madhusudhana, Effect of frequency of pulsing in gas tungsten arc welding on the microstructure and mechanical properties of titanium alloy welds, J. Mater. Sci. Lett. 15 (1996) 626–628.
[10] T.R. Tabrizi, M. Sabzi, S.H. Mousavi Anijdan, A.R. Eivani, N. Park, H.R. Jafarian, Comparing the effect of continuous and pulsed current in the GTAW process of AISI 316L stainless steel welded joint: microstructural evolution, phase equilibrium, mechanical properties and fracture mode, J. Mater. Res. Technol. 15 (2021) 199–212, https://doi.org/10.1016/j.jmrt.2021.07.154.
[11] M. Sabzi, S.H. Mousavi Anijdan, A.R. Bali Chalandar, N. Park, H.R. Jafarian, A.R. Eivani, An experimental investigation on the effect of gas tungsten arc welding current modes upon the microstructure, mechanical, and fractography properties of welded joints of two grades of AISI 316L and AISI310S alloy metal sheets, Materials Science and Engineering: A 840 (2022), https://doi.org/10.1016/j.msea.2022.142877.
[12] M. Sabzi, S.H. Mousavi Anijdan, A.R. Eivani, N. Park, H.R. Jafarian, The effect of pulse current changes in PCGTAW on microstructural evolution, drastic improvement in mechanical properties, and fracture mode of dissimilar welded joint of AISI 316L-AISI 310S stainless steels, Mat Sci EngA 823 (2021), https://doi.org/10.1016/j.msea.2021.141700.
[13] L. Zhao, X. Bai-lu, W. Shu-hui, D. Shan-xu, K. Yong, The sliding mode control for arc welding inverter power source, in: Proceedings of the IEEE ICIEA 2008, 2008, pp. 1100–1104, https://doi.org/10.1109/ICIEA.2008.4582688. Singapore.
[14] M. Wu, D. Flynn, A. Szymczak, Design and implementation of ZVZCS in full bridge DC/DC converter with digital control in arc welding machines application, in: Proceedings of the 2017 IEEE 26th International Symposium on Industrial Electronics, 2017, pp. 682–687, https://doi.org/10.1109/ISIE.2017.8001328. Edinburgh, UK.
[15] Q. Bellec, J.C. Le Claire, M.F. Benkhoris, P. Coulibaly, Power factor correction and DC voltage control limits for arc welding application using pulsed current, in: Proceedings of the IECON 2018, 2018, pp. 1406–1411, https://doi.org/10.1109/IECON.2018.8592678.
[16] A.K. Paul, Simple means of resolving issues of ac-tig welding equipment, in: Proceedings of the 2016 IEEE International Conference on Power Electronics, Drives and Energy Systems, Trivandrum, India, 2016, pp. 1–6, https://doi.org/10.1109/PEDES.2016.7914475.
[17] J.-M. Wang, S.-T. Wu, A novel inverter for arc welding machines, IEEE Trans. Ind. Electron. 62 (2015) 1431–1439, https://doi.org/10.1109/TIE.2014.2348942.
[18] B. Babes, A. Boutaghane, N. Hamouda, A novel nature-inspired maximum power point tracking (MPPT) controller based on ACO-ANN algorithm for photovoltaic (PV) system fed arc welding machines, Neural Comput. Appl. 34 (2022) 299–317, https://doi.org/10.1007/s00521-021-06393-w.
[19] A. Bouafassa, L.M. Fernández Ramírez, B. Babes, Power quality improvements of arc welding power supplies by modified bridgeless SEPIC PFC converter, J Power Electronics 20 (2020) 1445–1455, https://doi.org/10.1007/s43236-020-00143-2.
[20] O.F. Benaoudac, B. Babes, M. Bouchakour, S. Kahla, A. Bendiabdellah, Arc welding current control using thyristor based three-phase rectifiers applied to gas metal arc welding connected to grid network, J. Eur. Systèmes Automatisés 54 (2) (2021) 335–344, https://doi.org/10.18280/JESA.540216. April.
[21] A. Navarro, V.M. López, R. Casanueva, F.J. Azcondo, Digital control for an arc welding machine based on resonant converters and synchronous rectification, IEEE Trans. Ind. Inf. 9 (2013) 839–847, https://doi.org/10.1109/TII.2012.2222651.
[22] D. Czarkowski, M.K. Kazimierczuk, Phase-controlled series-parallel resonant converter, IEEE Trans. Power Electron. 8 (1993) 309–319, https://doi.org/10.1109/63.233288.
[23] R. Casanueva, F.J. Azcondo, F.J. Diaz, C. Branas, Teaching resonant converters: properties and applications for variable loads, IEEE Trans. Ind. Electron. 57 (2010) 3355–3363, https://doi.org/10.1109/TIE.2010.2045993.
[24] C. Brañas, F.J. Azcondo, R. Casanueva, F.J. Díaz, Pulsed Current Source with Active Control of the On-Time Current for LED Lamp Driver Applications, Proceeding of the IEEE IECON 2014, Dallas, TX, USA, 2014, pp. 1727–1732, https://doi.org/10.1109/IECON.2014.7048735.
[25] A.K. Singh, V. Dey, R.N. Rai, Techniques to improve weld penetration in TIG welding (A review), Mater. Today: Proc. 4 (2017) 1252–1259, https://doi.org/10.1016/j.matpr.2017.01.145.
[26] ASTM E8/E8M-16a, Standard Test Methods for Tension Testing of Metallic Materials, ASTM International, West Conshohocken, PA, 2016.
[27] ASTM E23-16b, Standard Test Methods for Notched Bar Impact Testing of Metallic Materials, ASTM International, West Conshohocken, PA, 2016.
[28] J.R. Davis (Ed.), ASM Specialty Handbook: Stainless Steels, Publisher: ASM International, Published, 1994, p. 576. ISBN: 978-0-87170-503-7.
[29] R. Scott Funderburk, A look of heat input, Welding Innovation 16 (1999) 1.
[30] N.T. Kottegoda, R. Rosso, Applied Statistics for Civil and Environmental Engineers, second ed., Blackwell Pub., Oxford, UK, 2008.
[31] W. Oldfield, Curve Fitting Impact Test Data: a Statistical Procedure, vol. 3, ASTM Stand. News, 1975, p. 11. United States.